# ATTITUDE CONTROL OF SMALL SATELLITES USING THRUSTER SYSTEMS

J. Schlutz

Universität Stuttgart / University of Sydney
Institut für Raumfahrtsysteme, Pfaffenwaldring 31, D-70550 Stuttgart

## ABSTRACT

The work presented here aims at identifying and describing the possibilities of active attitude control techniques on small satellites, focusing on the use of thruster actuation systems. A capable simulation environment has been developed in Matlab/Simulink, allowing investigation of complete attitude control scenarios. Different control approaches, their customisation for the mission specific attitude requirements, and stability considerations are shown.

Simulation results for two small satellite missions, the CASsat and the SSETI EXPRESS projects, provide a comparison of different controllers, thruster systems and arrangements, as well as verification and proof of flexibility of the implemented simulator.

## 1  INTRODUCTION

Small satellite systems, usually classified as micro-, nano- or even pico-satellites, have become of great interest within the last years, providing excellent educational and scientific opportunities of space access for research institutions and universities all over the world. Due to their size, mass, resources and cost restrictions those missions are especially challenging, often relying on not-yet space qualified hardware and technology.

One of the main challenges in satellite operations is the attitude and orbit control system, assuring that the spacecraft can fulfil its mission objectives throughout its lifetime. These control systems, in general consisting of sensors for attitude determination, an on-board data processing unit and actuators for active attitude control, depend highly on the mission scenario and requirements as well as the size and mass of the spacecraft itself. Both sensors and actuators have to be sized according to accuracies defined by communication and operational requirements, i.e. pointing for up- and downlink communication, scientific measurements, etc. One possibility of actuation are thruster systems with appropriate control loop design .

An orbit and attitude simulator has been developed and implemented using Matlab/Simulink and allows investigation of complete attitude control scenarios including detumbling as well as attitude acquisition and stabilisation. Due to its modular design and parameterised implementation the simulator allows testing of different satellite systems, control approaches and actuation systems for low Earth orbits. Its use has been simplified by the implementation of a graphical user interface for initialisation of the simulation parameters.

These simulation capabilities are demonstrated using data for two educational small satellite projects: the CASsat CubeSat project of the Centre of Excellence for Autonomous Systems (CAS), Sydney, using Pulsed Plasma Thruster technology, and the SSETI Express mission of the Student Space and Technology Initiative (SSETI) with a four thruster cold gas system. The main characteristics of those missions are summarised in TABLE 1.

This paper provides an executive summary of [1], for further details the reader is referred to this document.
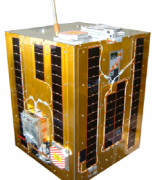
| | *CASsat* | *SSETI EXPRESS* |
|---|---|---|
| |  Example of Standard CubeSat (Cal Poly: CP1) |  |
| Size [mm$^3$] | 100 x 100 x 100 | 500 x 500 x 651 |
| Mass [kg] | 1 | 75 |
| Orbit | 800 km polar sun-synchronous i=98.73°, T=6070 s | 680 km polar sun-synchronous i=98.18°, T=5900 s |
| Mission | • radiometer payload • technology demonstration | • 3 CubeSats • technology demonstration • camera |
| Launch | TBC | 27.10.2005 |
| Att. Sensors | • magnetometers • sun sensors | • magnetometers • sun sensors |
| Att. Actuators | • magnetorquer • PPTs (theor.) | • passive magnet + magnetorquer • cold gas thrusters |

TABLE 1: Characterics of the investigated small satellite systems

## 2  THE SIMULATOR

In order to successfully design, test and verify a controller design for satellite attitude stabilisation, adequate simulation capabilities can be used and have been used extensively throughout this work. Although attitude and orbit simulation are commercially available today, a requirement for the educational benefit of small satellite projects is the fundamental understanding of and direct interaction with the simulator. Therefore a complete attitude and orbit simulation environment has been created using Matlab/Simulink and has been customised

for the specific requirements and optimisation parameters of small satellite missions.

## 2.1 Simulation Environment

According to Kepler's laws and Newton's gravity a spacecraft will follow an elliptic, parabolic or hyperbolic trajectory in a two-body system, i.e. the satellite and a central body. However, the satellite's movement in space is influenced by a number of environmental perturbations, where forces cause deviations from these Kepler orbits and torques also interfere with the spacecraft's attitude and rotational motion.

The environmental forces implemented in the current simulator are the gravitational influences of the Earth (EGM96), atmospheric drag for altitudes up to 1000 km (Harris-Priester density model), solar radiation pressure from the sun, and third-body gravitation from the sun and the moon. Additionally a control force from thrusters can be used to actively control the satellite's orbit, yielding the total external force (1).

$$(1) \quad \begin{aligned} \vec{F} &= \left( \vec{F}_{grav} + \vec{F}_{drag} + \vec{F}_{solar} + \vec{F}_{sun} + \vec{F}_{moon} \right) + \vec{F}_{control} \\ &= \vec{F}_{dist} + \vec{F}_{control} \end{aligned}$$

Perturbation torques included in the simulation are the gravity gradient torque, the aerodynamic torque, the solar radiation pressure torque and the residual magnetic dipole. As above, control actuators can be used for active attitude control which will be presented in detail in chapters 3 and 4, resulting in an external torque as in (2).

$$(2) \quad \begin{aligned} \vec{T} &= \left( \vec{T}_{GG} + \vec{T}_{aero} + \vec{T}_{solar} + \vec{T}_{mag} \right) + \vec{T}_{control} \\ &= \vec{T}_{dist} + \vec{T}_{control} \end{aligned}$$

These perturbations represent the main contributors to the environmental effects. Other forces and torques also exist, but their influence can usually be neglected in low Earth orbit and they were therefore not implemented in the simulator to reduce computation time.

## 2.2 Equations of Motion

Heart of the implemented simulator is a 6-DOF-equations of motions block for the central integration, which calculates the new position, velocity, attitude and body rates of the spacecraft depending on external forces and torques as described above. It uses the standard equations of motion for orbit and rotational movement; those equations are given here without derivation [2],[3],[4]. While equations (3) and (4) describe the translational motion influenced by perturbation forces, equations (5) and (6) characterise dynamics and kinematics of the satellite's rotation.

$$(3) \quad \vec{F} = m \cdot \left( \dot{\vec{V}} + \vec{\omega} \times \vec{V} \right)$$

$$(4) \quad \dot{\vec{r}} = \vec{V}$$

$$(5) \quad \vec{T} = \dot{\vec{h}} + \vec{\omega} \times \vec{h} = \mathbf{I} \cdot \dot{\vec{\omega}} + \vec{\omega} \times \left( \mathbf{I} \cdot \vec{\omega} \right)$$

$$(6) \quad \underline{\dot{q}} = \frac{1}{2} \mathbf{\Omega}\left( \underline{q} \right) \cdot \vec{\omega} = \frac{1}{2} \begin{pmatrix} -q_1 & -q_2 & -q_3 \\ q_0 & -q_3 & q_2 \\ q_3 & q_0 & -q_1 \\ -q_2 & q_1 & q_0 \end{pmatrix} \cdot \begin{pmatrix} \omega_x \\ \omega_y \\ \omega_z \end{pmatrix}$$

Quaternions are implemented for attitude representation within the simulation due to their significant reduction in computation costs and the absence of singularities, but other representations such as Euler angles are used for better visualisation of the results.

The attitude equations are obviously non-linear; however, linearization is possible about a given set point. For the given satellite application the sensor axis is assumed to be the body z-axis and a nadir pointing attitude was chosen as reference attitude. Linearization of the kinematic and dynamic equations then yields the state space model (7).

$$(7) \quad \begin{aligned} \dot{\vec{x}} &= \mathbf{A} \cdot \vec{x} + \mathbf{B} \cdot \vec{u} = \mathbf{A} \cdot \begin{pmatrix} \Delta\vec{\omega} \\ \underline{q}_E \end{pmatrix} + \mathbf{B} \cdot \vec{T}_{control} \\ \vec{y} &= \mathbf{C} \cdot \vec{x} + \mathbf{D} \cdot \vec{u} = \mathbf{C} \cdot \begin{pmatrix} \Delta\vec{\omega} \\ \underline{q}_E \end{pmatrix} + \mathbf{D} \cdot \vec{T}_{control} \end{aligned}$$

$$\mathbf{A} = \begin{pmatrix} 0 & 0 & -\sigma_x\omega_0 & -6\sigma_x\omega_0^2 & 0 & 0 \\ 0 & 0 & 0 & 0 & 6\sigma_y\omega_0^2 & 0 \\ -\sigma_z\omega_0 & 0 & 0 & 0 & 0 & 0 \\ \frac{1}{2} & 0 & 0 & 0 & 0 & \frac{1}{2}\omega_0 \\ 0 & \frac{1}{2} & 0 & 0 & 0 & 0 \\ 0 & 0 & \frac{1}{2} & -\frac{1}{2}\omega_0 & 0 & 0 \end{pmatrix}$$

$$\mathbf{B} = \begin{pmatrix} \mathbf{I}^{-1} \\ \mathbf{0} \end{pmatrix} \qquad \mathbf{C} = \begin{pmatrix} \mathbf{0} & \mathbf{E} \end{pmatrix} \qquad \mathbf{D} = \mathbf{0}$$

This model is fully controllable and fully observable according to linear control theory.

$\underline{q}_E$ denotes the error quaternions to the reference attitude $\underline{q}_{ref}$ and $\Delta\vec{\omega}$ the corresponding rate deviation. The pointing requirements are usually formulated as maximum Euler angle deviations, for angles smaller than 10 degrees the corresponding quaternions can be approximated as (8).

$$(8) \quad \underline{q}_{max} = \begin{pmatrix} q_{max,0} \\ q_{max,1} \\ q_{max,2} \\ q_{max,3} \end{pmatrix} \approx \begin{pmatrix} 1 \\ \phi_{max}/2 \\ \theta_{max}/2 \\ \psi_{max}/2 \end{pmatrix} \qquad \underline{q}_{ref} = \begin{pmatrix} 1 \\ 0 \\ 0 \\ 0 \end{pmatrix}$$

## 2.3 Simulator Implementation

The simulator is implemented in the Matlab/Simulink environment, allowing a very modular program structure so that parts and models can be exchanged quickly if new data or procedures become available without the need for alteration of the whole system. Its central core is the equations of motions block and the calculations of perturbation and control actuations as shown in FIG. 1.

A graphical user interface for parameter initialisation has also been created to facilitate the use of the simulator,

while a VRML interface is used for visualisation during simulation runtime, FIG. 2.
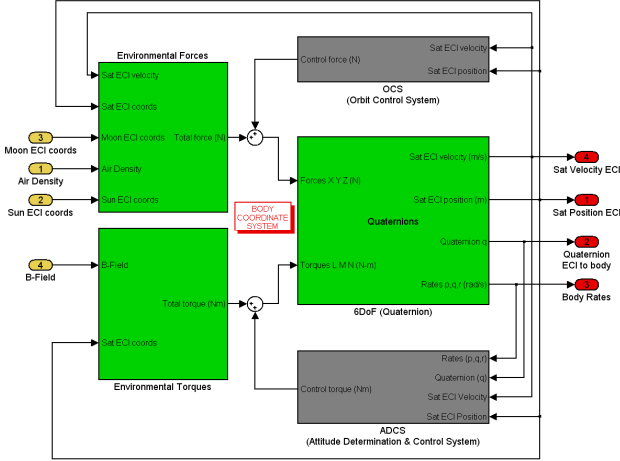


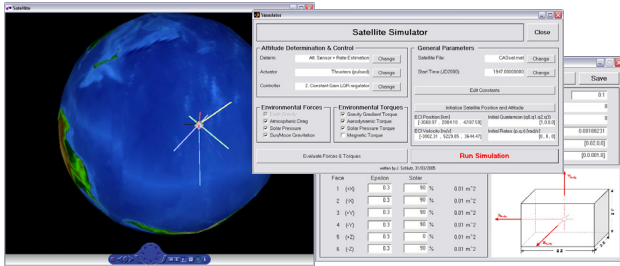FIG. 1: Central satellite motion block of the simulation



FIG. 2: VRML visualisation (left) and graphical user interface (right) of the developed simulator

## 3  THRUSTER SYSTEMS

Thrusters provide an already space-proven possibility for both attitude and orbit control of satellites. However, their implementation on small satellite systems still is a challenging task due to the generally complex system setup.

### 3.1  Thruster Systems Characteristics

A typical, single thruster is characterised by several parameters to outline its performance. Since a thruster relies on the exchange of momentum by exhaust of propellant, the most obvious parameter is of course the thrust force $F$ or the thrust $\vec{F}$. For typical small satellite attitude control applications this force is in the range of mN or even μN. Alternatively the mass specific impulse $I_{sp}$ is used for comparison between thrusters. Since the thrust force is directed, a torque about the centre of mass is generated if the line of action does not run through the centre of mass. This torque, calculated as the cross product of the thrust and the thruster position vector, is used for attitude actuation. A setup of several thrusters is then referred to as a thruster system for attitude control.

A minimum set of four thrusters – if adequately positioned on the spacecraft – is necessary for full three axis control. For such a system of n thrusters all single thruster torques can be summarized in a torque matrix (9).

$$(9) \qquad \mathbf{A_{th}} = \begin{pmatrix} \vec{T}_{th,1} & \vec{T}_{th,2} & \cdots & \vec{T}_{th,n} \end{pmatrix}$$

$$(10) \qquad \vec{T}_{control} = \mathbf{A_{th}} \cdot \vec{f}_{sys}$$

This allows calculation of the applied control torque from equation (10) where $\vec{f}_{sys}$ is a vector of binary on-off signals for the thrusters. This also defines only certain achievable control torque magnitudes and directions depending on the actual thruster system setup. The commanded torque can therefore not be exactly matched by the thruster setup at any time, but the closest solution is chosen. However, the important control problem is the calculation of those on-off signals from the commanded torque. Since the matrix $\mathbf{A_{th}}$ is not quadratic it cannot be inverted, but a pseudo-inverse matrix can be calculated using singular value decomposition (SVD). This yields (11) with the actuation matrix $\mathbf{A_{th}^I}$.

$$(11) \qquad \vec{f}'_{sys} = \mathbf{A_{th}^I} \cdot \vec{T}_{com}$$

Calculations using equation (11) can result in negative elements in the thruster signals $\vec{f}'_{sys}$. As this is not possible, the correct orientation of the thrust signal has to be assured. This is achieved by an additional nullspace component that can be defined for the thruster system [5]. The nullspace refers to a thruster actuation signal $\vec{f}_{null}$ that does not generate a torque about any spacecraft axis, i.e. (12).

$$(12) \qquad \vec{T}_{control} = \mathbf{A_{th}} \cdot \vec{f}_{null} = 0$$

Adding this nullspace component to the above actuation signal calculated from the commanded torque can then be used to assure only positive elements in $\vec{f}_{sys}$ while not changing the generated control torque.

$$(13) \qquad \vec{f}_{sys} = \mathbf{A_{th}^I} \cdot \vec{T}_{com} - \sum_i u_i \vec{f}_{null,i} \quad i = 1,\ldots,n_{nullspace}$$

Since no thruster can appear on its own in a nullspace signal and every single thruster should appear in only one nullspace signal, there exist between 1 and n/2 nullspace vectors depending on the thruster system setup. Each of these nullspace signals $\vec{f}_{null,i}$ has to be subtracted from the solution with the appropriate command $u_i$ to ensure a positive command signal for every thruster (13).

This can most easily be visualized by two opposing thrusters, i.e. they are mounted at the same position, but with opposite thrust directions. They generate the same magnitude of control torque, but with opposing sign. An actuation of both thrusters at the same time will therefore not result in any attitude movement, this is a nullspace actuation. If a negative actuation signal is calculated for one of the thrusters, this torque can easily be generated by firing the other, or mathematically by adding the appropriate nullspace component to the overall actuation signal.

The problem in the control actuation is to find the appropriate nullspace command $u_i$ for each nullspace vector. It is given by the minimum calculated control signal for the thrusters contributing to the nullspace vector.

$$(14) \qquad u_i = \min_j \left( \vec{f}'_{sys} \right)_j = \min_j \left( \mathbf{A^I_{th}} \cdot \vec{T}_{com} \right)_j$$

where j are the indices of the non-zero elements in $\vec{f}_{null,i}$.
This also eliminates any unnecessary thruster actuation (e.g. firing of both the two opposing thruster from the earlier example), thus minimising fuel and power consumption.

Another characteristic of a thruster system is its system torque $\vec{T}_{sys}$, which we define as the (maximum) torque magnitude about each body axis. It can be given by the sum of the thruster torques producing a positive torque about a spacecraft axis without generating a torque about any of the other two axes.

A thruster system is now characterised by

- the number of thrusters, n. with their corresponding forces, impulse bits and torques,
- the torque matrix $\mathbf{A_{th}}$ and the actuation matrix $\mathbf{A^I_{th}}$,
- the system torque $\vec{T}_{sys}$,
- its nullspace actuation signals, $\vec{f}_{null,i}$.

## 3.2 Limitations of Thruster Systems

Thrusters can easily be positioned adequately on a spacecraft to ensure full three axes control capability, but they still face other design and performance limitations.

Since thrusters can generally not be throttled, on of these constraints is a certain torque $\vec{T}_{sys}$ about each body axis and a minimum firing time $\tau$ of the thrusters themselves, due to e.g. valve opening/closing times, electric delay, etc. This limits the minimum angular velocity change of the spacecraft to

$$(15) \qquad \Delta \vec{\omega}_{min} = \dot{\vec{\omega}} \cdot \tau = \mathbf{I}^{-1} \vec{T}_{sys} \cdot \tau$$

For attitude acquisition and stabilisation this becomes evident in the fact that the optimum desired attitude can generally not be achieved, but only a limit cycle about this orientation. In the case of stabilisation of the satellite with respect to inertial space (or very small angular velocities) the attitude motions about the three principal axes are nearly uncoupled, i.e. the cross product can be neglected and the movement about each axis may be treated separately. The Euler angles equation (5) then becomes (for each axis)

$$(16) \qquad \ddot{\varphi} = \frac{d\dot{\varphi}}{d\varphi} \dot{\varphi} = \frac{T}{I_i} \;\; \rightarrow \;\; \dot{\varphi}^2 = \dot{\varphi}_0^2 + 2\frac{T}{I_i}\left(\varphi - \varphi_0\right)$$

This means that the angular acceleration about each axis is zero in the absence of external torques and constant for a constant torque, describing the rotational motion as a parabolic trajectory in the $\varphi, \dot{\varphi}$-phase diagram. In the vicinity of the equilibrium attitude ( $\varphi = \dot{\varphi} = 0$ ) the satellite's movement about each axis therefore results in a hard limit cycle in the absence of disturbance torques or in a soft limit cycle as shown in FIG. 3.
Once the attitude is within the specified limits the thruster system is only used to maintain those limits. FIG. 3 (left) shows a symmetric limit-cycle where the drift rate is half

the angular velocity change achieved by the thruster. This is generally not the case since the attitude has to be reached with an acquisition manoeuvre from an arbitrary position in space, therefore, the magnitudes of the positive and negative drift velocities can differ, but will always be smaller than $\Delta\omega_{thrust}$.
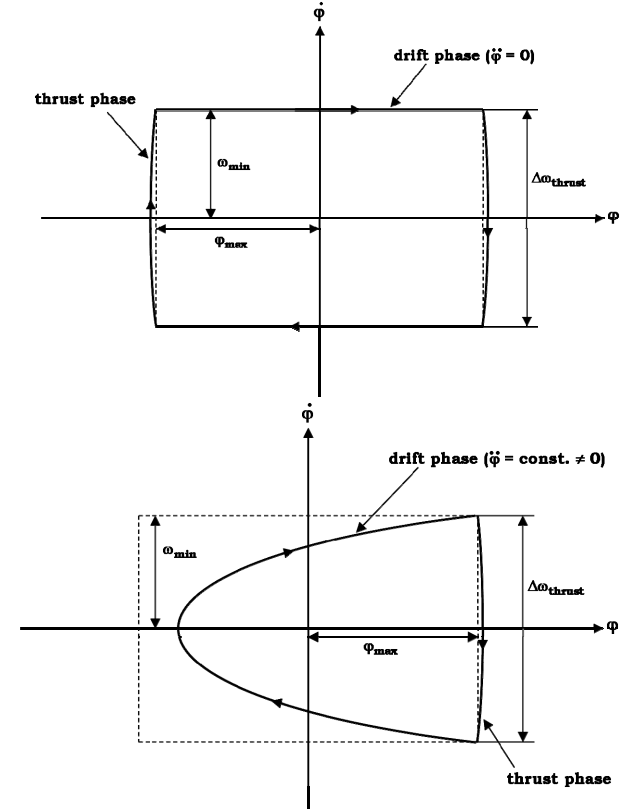


FIG. 3: Hard (top) and soft limit cycle around the reference attitude during attitude stabilisation

In the presence of disturbance torques this limit cycle obviously changes since $\ddot{\varphi}$ is no longer zero during the drift phase. In an adequately proportioned control system, the constant disturbance torque dictates the satellite movement during the drift phase, the thruster actuation is only necessary to assure the attitude stabilisation within the specified limits. In reality the disturbance torque will not be constant, but it can usually be approximated like that between two consecutive thruster firings. However, its magnitude will vary, resulting in a variation of thruster actuation frequency. It can be seen that thruster activation might actually be reduced in the presence of disturbance torques since only one reversing of angular velocities is necessary, however, this requires very accurate thruster system design and cannot account for uncertainties in the environmental torques.

## 3.3 Thruster Systems Hardware

### 3.3.1 Pulsed Plasma Thrusters (PPT)

Due to the miniaturization of space missions and advance in technology and reliability, electrical thrusters have become of great interest throughout the years. Their high efficiencies and low propellant consumption allow smaller and lighter propulsion systems especially for long

duration missions where the increase in necessary power and therefore power system mass is small compared to the amount of propellant needed in chemical thrusters.
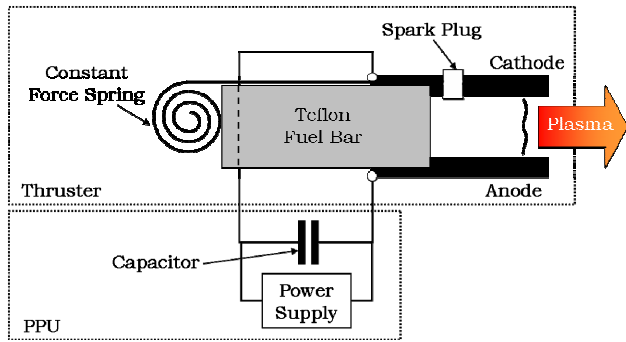


FIG. 4: Basic scheme of a pulsed plasma thruster

One of those electrical thruster systems is the Pulsed Plasma Thruster (PPT). The thrusters themselves have been extensively studied and qualified for space on several missions, namely the Russian Zond-2 spacecraft in 1964 and the US LES-6 (1970), NOVA (1981,1983) and EO-1 (2000) satellites. Recently interest has grown in the miniaturization of those propulsion systems and their usage on small satellite missions [6],[7]. A recent study at the University of Sydney also aims at developing a miniature PPT system for nano- or pico-satellite applications, especially a possible use of those thrusters on the CASsat mission [8].

A pulsed plasma thruster uses a solid propellant source, most often Teflon, that is ablated by a high discharge current and accelerated by electromagnetic and gas dynamic pressure forces. It can be divided into the thruster itself and a power processing unit (PPU), generating the necessary discharge current and voltage. Since this is a small and self-contained propulsion system it allows simple integration into the satellite. A very basic scheme of a pulsed plasma thruster unit can be seen in FIG. 4. The use of a solid propellant like Teflon makes the PPT design very simple since no moving parts are required except for the constant force spring and it facilitates miniaturization for small satellites. Since Teflon also has the advantage of being non-toxic and inert it also is one of the safest propulsion systems and does not violate the CubeSat standards.

The main characteristics of the PPT system used in the CASsat simulation are summarised in TABLE 2.

### 3.3.2 Cold-gas Propulsion

A cold gas system is one of the simplest propulsion systems and has been used for attitude control for decades. Its principle is to expel a gaseous propellant through a thruster nozzle, thus producing a thrust force acting on the spacecraft due to the exchange of momentum. The propellant is stored in a tank and fed to the thruster via a system of tubing, pressure regulators and valves. There is a long list of flight heritage, one of the latest projects is the European CryoSat mission due for launch this year.

The mass specific impulse bit of a cold gas system is highly dependent on the propellant, most commonly nitrogen is used with an $I_{sp}$ of about 60 to 70 s. This also limits the thrust level and cold gas thrusters have been

built with a thrust force ranging from several hundred mN up to some N.
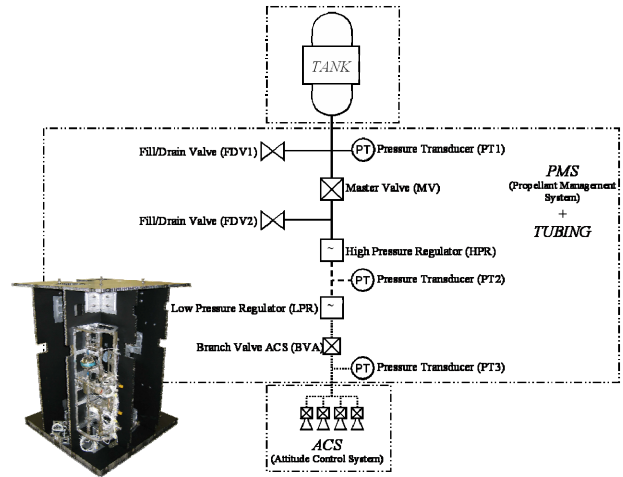


FIG. 5: Scheme and picture of the SSETI EXPRESS cold gas propulsion unit

One of the major decision factors for the cold gas system within the SSETI project was its simplicity and use of non-toxic propellant allowing hands-on experience and testing for the students themselves. Four thrusters with conical nozzles producing a thrust of 130 mN each are used to generate torques about all three spacecraft axes. The scheme of the SSETI Express propulsion system and a picture of the integrated propulsion components in the SSETI Express structure can be seen in FIG. 5, while TABLE 2 summarises the thruster characteristics [9].

| | PPT (CASsat) | Cold-gas (SSETI EXPRESS) |
|---|---|---|
| Thrust | 100 μN | 130 mN |
| Firing time | 10 ms | >20 ms |
| Min. impulse bit | 1 μNs | 2.6 mNs |
| Specific impulse | 500 s | 65 s |

TABLE 2: Characteristics of the pulsed plasma thruster (PPT) and cold-gas propulsion systems as used for the simulation

### 3.4 Thruster Configurations

As described earlier a minimum of four thrusters is necessary for full 3-axis attitude control in order to create at least one nullspace to ensure positive thruster actuation signals. Different thruster configurations with between four and twelve thrusters have been developed and compared using the simulator and the CASsat PPTs. Each configuration has advantages and disadvantages due to the achievable torque levels, independent axes control possibilities, and the available satellite resources.
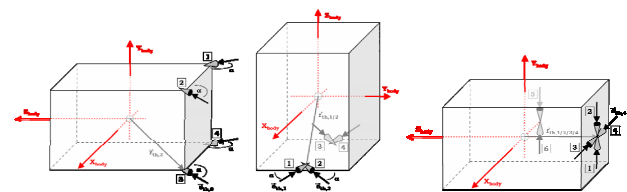


FIG. 6: "4-Force" (left), "4-SSETI" (middle), and "6-Indep" thruster configurations for the simulation

The four thruster "4-Force" configuration was chosen as most promising approach for the CASsat mission due to the stringent size and mass constraints, while the "6-Indep" setup was extensively used in the simulation due to its simple torque actuation. The SSETI EXPRESS satellite uses a four thruster configuration titled "4-SSETI" within this work.

### 3.5 Thruster Modelling and Implementation

The PPTs and the cold-gas system have to be represented in the simulator to allow investigation of the 3-axis control capabilities. The controller output is a commanded torque signal, which is then distributed to the single thrusters using the actuation matrix. A thruster is only activated if the commanded torque exceeds its specific thruster torque, resulting in a deadband as described later in the controller design.

The PPTs can only be fired at a specific impulse bit and frequency, allowing very simple implementation in the simulator in the form of effective torques per second. The simulation results therefore show consecutive thruster pulsing as continuous actuation.

Thruster systems such as the cold gas or chemical propulsion units have a minimum impulse bit due to valve response and operating times, however, they can be fired continuously to a certain extent. The quasi-continuous actuation signal therefore has to be transformed into an on/off pulse train for each thruster. For this purpose so-called modulators are used. The pulse width modulator (PWM) is a fixed frequency device. It uses a fixed sample period (here 1 Hz due to sensor sampling time). Every time step gives a calculated actuation signal for each thruster, the pulse length is then varied according to the magnitude of the calculated actuation signal (FIG. 7).
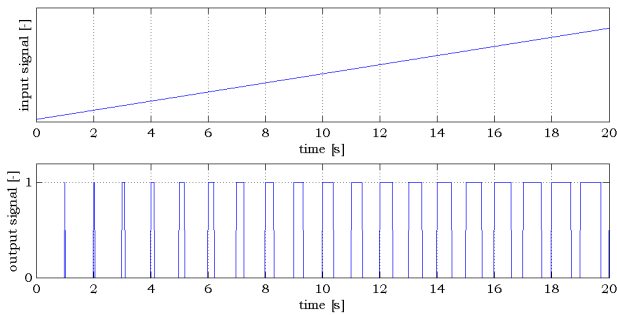


FIG. 7: Pulse width modulation of a simple ramp input

## 4 ATTITUDE DETERMINATION AND CONTROL

The function of the attitude determination and control system (ADCS) is to measure, compute and adjust the spacecraft's attitude throughout the whole mission, thus enabling the achievement of mission objectives depending on this stabilisation. The system therefore generally comprises three parts as illustrated in FIG. 8:

- attitude determination (sensors) for measurement
- attitude controller for computation and command
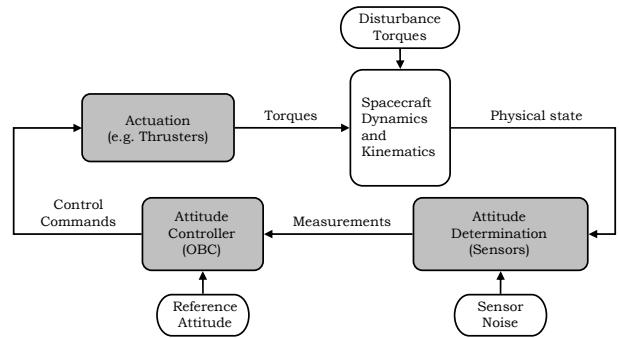- actuators for active attitude control



FIG. 8: Basic scheme of an attitude determination and control system

### 4.1 Attitude Determination and Control Hardware

Many different types of ADCS hardware have been developed and successfully qualified in space, both for determination and actuation.

Measurement of the attitude and the body rates is necessary for full rotational information. Sensor concepts for these applications include sun sensors, Earth sensors, star trackers, magnetometers and gyroscopes. A combination of these devices is generally used depending on the pointing requirements and spacecraft resources. As shown in TABLE 1 and mathematically described in (7) both investigated satellites do not have gyroscopes for rate measurements; however, this information can be estimated from attitude measurements which has been demonstrated in the simulation environment.

Space qualified actuation hardware on satellites are thrusters, magnetorquers and wheel devices. This work focuses on the use of thruster systems, more information on magnetic actuation for small satellite application can be found in [10].

### 4.2 Controller Design

The attitude controller has to assure correct orientation and rotation of the spacecraft throughout its operational mission phase, which usually characterised by different operational and scientific requirements. Therefore, different control laws can be used to optimise the spacecraft motion for each application. They provide the main possibility for the engineer to influence the attitude control performance characteristics and to assure stability of the control loop.

All following calculations and considerations are formulated in the satellite's body coordinate system, representing its principal axes.

#### 4.2.1 Rate Control

After separation from the launch vehicle or re-activation the spacecraft might rotate at an arbitrary rate about its body axes. The objective of the rate controller (or detumbling controller) therefore is to reduce the angular velocities about all body axes with respect to the inertial frame to a value that allows and ensures active attitude control using the controller for nominal operation, i.e. attitude acquisition and stabilisation.

Since only the body rates are controlled and not the attitude, only the rates need to be fed back in the regulator design. The control law therefore simply becomes

$$(17) \qquad \vec{T}_{com} = -K_{det} \cdot \vec{\omega}$$

Here, $\vec{T}_{com}$ denotes the calculated control torque that is commanded to the thruster actuation system. Due to constraints in the thruster system this might differ from the actually generated control torque $\vec{T}_{control}$, this actuation is described in 3. Asymptotic stability of this control law in the non-linear satellite motion can be shown using Lyapunov theory according to [5],[12] for any positive definite gain matrix $K_{det}$. This feedback matrix is simply chosen as a diagonal matrix

$$(18) \qquad K_{det} = \begin{pmatrix} k_{det,x} & 0 & 0 \\ 0 & k_{det,y} & 0 \\ 0 & 0 & k_{det,z} \end{pmatrix} \quad K_{det} > 0$$

$$(19) \qquad \frac{T_{sys,i}}{\omega_{max,i}} \le k_{det,i} \le \frac{2 \cdot T_{sys,i}}{\Delta\omega_{min,i}} = \frac{2 \cdot I_i}{\tau} \qquad i = x, y, z$$

The hardware limitations (15) of the thruster system together with the target rate $\vec{\omega}_{max}$ for detumbling yield an interval for the values of the gain matrix as in (19). The actually implemented value usually is close to the lower limit of this band since any body rate larger than the target rate shall trigger a thruster actuation while minimising total firings and thus fuel consumption.

### 4.2.2 Linear Switching Function

The most simple form of the linear switching function results in the control law (20), where the sign of the control torque is simply switched according to the current attitude and rate information.

$$(20) \qquad T_{com,i} = -T_{sys,i} \cdot sign(\varphi + const. \cdot \dot{\varphi}) \quad i = x, y, z$$
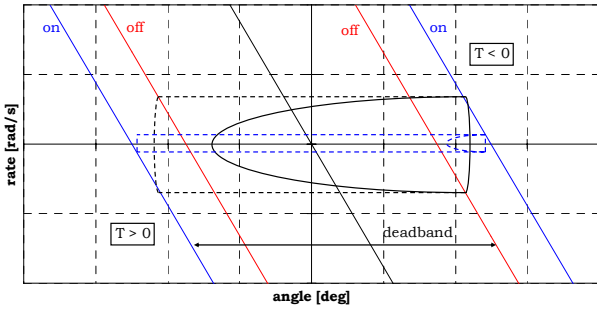


FIG. 9: Simple linear switching function (black), linear switching with deadband (blue) and Schmitt trigger (blue+red)

However, this will lead to a jitter about the equilibrium attitude wasting thruster propellant. A "deadband" is therefore introduced to limit thruster activation and define the already described limit cycle (FIG. 9). The re-written control law then becomes (21) with the yet to be defined feedback matrices $K_d, K_p$.

$$(21) \qquad \vec{T}_{com} = -K_d \Delta\vec{\omega} - K_p \vec{q}_E$$

Asymptotic stability can be shown using Lyapunov theory for a positive definite diagonal matrix $K_d$, a scaled unity matrix $K_p$, and inertial body rate feed back. The desired nadir pointing mode is not an inertial mode, however, linear control theory using the state space model (7) and simulations also shows stability of the above control approach.

$$(22) \qquad K_d = \begin{pmatrix} k_{d,x} & 0 & 0 \\ 0 & k_{d,y} & 0 \\ 0 & 0 & k_{d,z} \end{pmatrix} \quad K_p = k_p E \quad K_d, K_p > 0$$

Main objective of the controller is to drive the satellite attitude within the specified limits, therefore, any deviation from this attitude should trigger a corresponding thruster activation, regardless of the angular velocity. This yields (23) and also defines the controller deadband (24).

$$(23) \qquad k_p \ge max\left(\frac{T_{sys,i}}{q_{max,i}}\right) \qquad i = x, y, z$$

$$(24) \qquad deadband\Big|_i = \frac{T_{sys,i}}{k_p} \le 2q_{max,i} \qquad i = x, y, z$$

The thruster system can only provide a maximum angular velocity change within the pointing limits as calculated in equation (25). This and the minimum velocity change described earlier provide an interval for the derivative feedback values shown in (26). The lower limit is usually chosen to assure acquisition within the pointing limits and to avoid unnecessary thruster actuation.

$$(25) \qquad \Delta\omega_{max,i} = \sqrt{\frac{2T_{sys,i}}{I_i} \cdot \varphi_{max,i}} \qquad i = x, y, z$$

$$(26) \qquad \frac{T_{sys,i}}{\Delta\omega_{max,i}} \le k_{d,i} \le \frac{T_{sys,i}}{\Delta\omega_{min,i}} = \frac{I_i}{\tau} \qquad i = x, y, z$$

For small values of the rate feedback gains the body rates can actually get very high for large angle manoeuvres, making it impossible for the thruster system not to overshoot the desired attitude. This can be avoided by limiting the attitude feedback, i.e. introducing a limiter for each axis, limiting the magnitude of the quaternion element as given in (27),(28).

$$(27) \qquad \vec{T}_{com} = -K_d \Delta\vec{\omega} - K_p \cdot L_p(\vec{q}_E)$$

$$(28) \qquad L_p(q_i) = \begin{cases} q_i, & if \; |q_i| < L_{p,max} \\ \\ sign(q_i) \cdot L_{p,max}, & if \; |q_i| \ge L_{p,max} \end{cases} \quad i = 1,2,3$$

$$(29) \qquad |\Delta\omega_{\infty,i}| = \frac{1}{k_{d,i}}\left(T_{sys,i} + k_p L_{p,max}\right) \qquad i = x, y, z$$

The parameter $L_{p,max}$ can then be used to design the steady state rate for large angle rotations according to (29). Another approach in optimisation of final attitude motion might be the implementation of a Schmitt trigger, resulting in longer thruster burn times to adjust the limit

cycle as shown in FIG. 9. However, simulations showed no reduction of total thruster actuation using this principle.

### 4.2.3 Quadratic Switching Function

It has been shown that the satellite's rotational motion about each principal axis follows a parabolic trajectory when plotting rates $\dot{\varphi}$ versus the attitude angle $\varphi$ (FIG. 10). Therefore, a quadratic switching function suggests itself in order to minimise acquisition time and to avoid oscillations. It can be formulated with a deadband as

$$(30) \quad \vec{T}_{com} = -\mathbf{K_p}\vec{q}_E - \mathbf{K_d} \cdot \text{diag}(\Delta\vec{\omega})^2 \cdot \text{sign}(\Delta\vec{\omega})$$

Stability considerations for this controller can be done exactly as for the linear switching function. Lyapunov theory shows asymptotic stability for inertial rates and stability for the nadir pointing mode is given via linear control theory.

The condition for the proportional feedback (23) still hold, while similar consideration for the derivative gain yield

$$(31) \quad k_{d,i} \geq \frac{T_{sys,i}}{\Delta\omega_{max,i}^2} = \frac{I_i}{2 \cdot \varphi_{max,i}} \qquad i = x, y, z$$

A limiter is not necessary for this controller as it uses the capabilities of the actuation system already in the design. However, as for the linear switching function, calculation of the feedback gains is independent of the actuation type and universal for a certain satellite and mission.
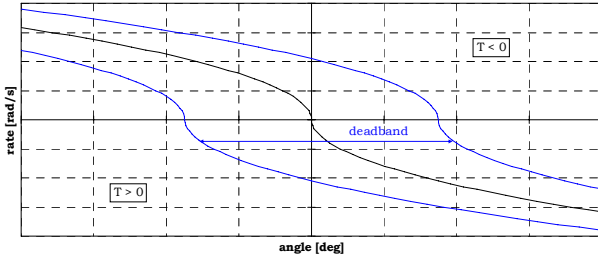


FIG. 10: Quadratic switching function and deadband

### 4.2.4 Linear Quadratic Regulator

Since linearization of the equations of motion about the nadir pointing position is possible, the use of linear control theory is another possibility for the attitude stabilisation. Therefore a linear quadratic regulator (LQR) has been designed and its performance compared to the above mentioned controllers. The linear quadratic regulator design uses the minimisation of the weighted state deviations to find a controller that increases stability and damping [13]. It reduces those deviations as fast as possible while at the same time minimising the control actuation. The control law is given by (32), where $\mathbf{P}$ is the solution of the algebraic Riccati equation (33).

$$(32) \quad \vec{T}_{com} = -\mathbf{K}_{SVF}\vec{x} \qquad \mathbf{K}_{SVF} = -\mathbf{R}^{-1}\mathbf{B}^T\mathbf{P}$$

$$(33) \quad \mathbf{A}^T\mathbf{P} + \mathbf{PA} - \mathbf{PBR}^{-1}\mathbf{B}^T\mathbf{P} + \mathbf{Q} = 0$$

Simulations also showed stability for this control approach, however, it has to be stated that the controller itself depends on the linearization and thus on the satellite orbit and reference attitude, therefore it has to be re-designed for a changed orbit.

## 5 SIMULATION RESULTS

### 5.1 CASsat Simulation

#### 5.1.1 Rate Control

Initial attitude and rate information is and will not be known for any satellite mission. However, the CubeSat deployment mechanisms specify angular velocities of 0.1 rad/s or less about each body axis, which was used as initial values for the simulation. The target rate for the detumbling controller was set to 0.001 rad/s about each body axis.

All thruster configurations successfully reduce the angular velocities of the satellite below the desired value as expected; they only differ in the necessary time and thruster activations as shown in FIG. 11. This is evident due to the different thrust and torque levels generated. Since the effective thruster torques are more than a factor of ten higher than the disturbance torques the latter have only little influence on the detumbling process itself.

The simulations show that detumbling is possible for all thruster configurations and in the presence of disturbance torques. The number of thruster firings is very large at about 10000 to 17000, thus requiring large resources in terms of power and a high reliability and reproducibility of the pulsed plasma thrusters. However, PPT systems have been tested in long-term experiments and demonstrated life to about 20 million pulses. With the CASsat PPT characteristics the necessary propellant adds up to only about 0.0036 g, while the power demand reaches up to about 180 Ws.
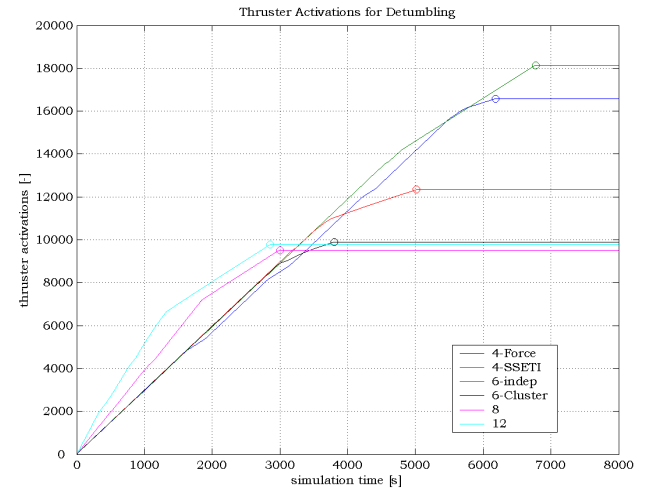


FIG. 11: Thruster activation and detumbling time for different thruster configurations during CASsat rate control

#### 5.1.2 Attitude Acquisition and Stabilisation

Comparison of the different control approaches has been performed using the 6-Indep PPT configuration. The initial pointing requirement of the CASsat mission is 5 degrees on all axes. As expected, successful acquisition and stabilisation was possible for all controllers. Simulations also showed the possibility of increased attitude accuracy better than 1 degree without increasing the necessary thruster actuations.
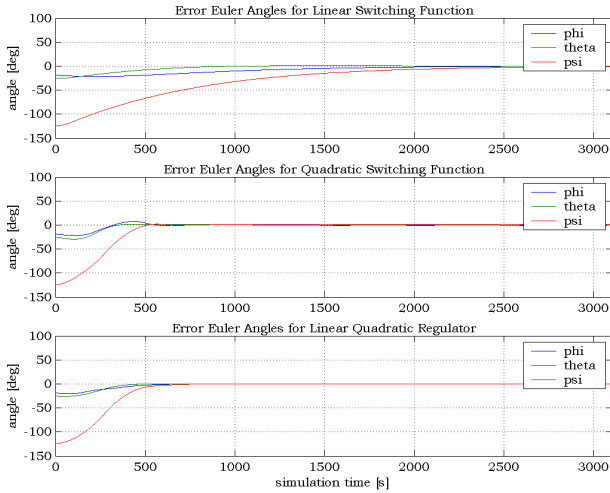
FIG. 12: Comparison of attitude acquisition with different control laws for the CASsat 6-Indep PPT configuration

An acquisition manoeuvre is shown for each controller in FIG. 12. All manoeuvres have been optimised in the control gains or with a limiter in order to avoid overshooting. While the linear switching function minimises control actuation (451 firings), it needs a long acquisition time of about 3000 s. The quadratic switching function minimises the acquisition time to only 600 s, but control actuations add up to about 1400 firings. The linear quadratic regulator provides a good compromise between both with acquisition within 720 s at about 950 thruster firings. Due to this and the low computational effort on-board, the linear quadratic regulator was selected as baseline controller for the CASsat.

### 5.1.3 Thruster Configurations

Based on this LQR design the different thruster configurations have been tested in the simulation environment. All thruster system setups achieved acquisition to the nadir reference within the required limit of 5 degrees on all axes after less than about 700 s (FIG. 13).
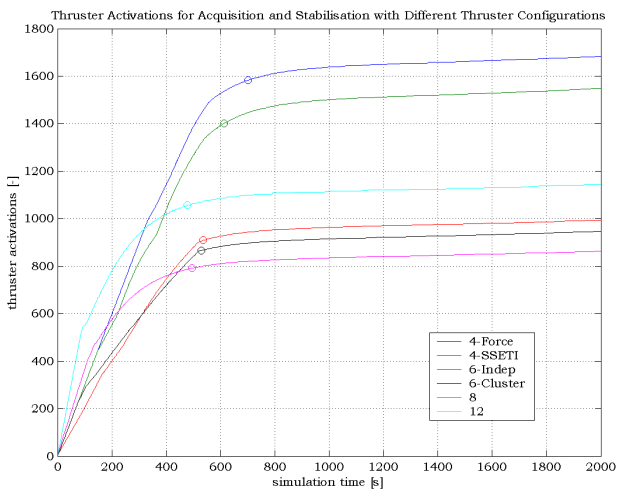


FIG. 13: Thruster activations and acquisition time with different PPT configurations on the CASsat mission

The rotational motion had no overshooting, however, the thruster systems showed some differences. Naturally the

configurations with more thrusters achieved faster acquisition because of the higher system torque level, however, the difference in acquisition time was not as significant as expected. This is due to the still very low torque of the PPT propulsion units in general.

The simulations show that a low mass system using only four thrusters can still achieve very accurate pointing and stabilisation with a slightly higher control actuation. The 6-Indep configuration is optimal with regard to pointing accuracy at little thruster activation since it provides the smallest system torque, however, larger numbers might be considered due to redundancy and faster detumbling and attitude acquisition.

### 5.1.4 CASsat Mission Scenario

The last sections discussed performance characteristics of different control approaches as well as thruster configurations for the CASsat pico-satellite. This chapter shows a complete mission scenario for the CASsat spacecraft using the 4-Force configuration The detumbling controller as presented in 4.2.1 is used as well as the linear quadratic regulator for attitude acquisition and stabilisation after successful rate control.

The spacecraft is assumed to be separated from the launch vehicle at the start of the simulation, floating at an arbitrary attitude with angular rates up to 0.1 rad/s about all body axes. Due to safety regulations the satellite is activated about five minutes after deployment when the detumbling controller is activated as well. As soon as all inertial body rates fall below the specified value of 0.001 rad/s, the ADCS switches to the LQR controller for final attitude acquisition, which is then stabilised throughout the rest of the simulation.

The developing of the attitude and rates with respect to the reference nadir frame can be seen in FIG. 14. The thruster system starts pulsing after 300 s as specified. The angular velocities are then successfully reduced after about 6500 s. The acquisition controller rotates the spacecraft to its desired nadir pointing orientation within 815 s using 1210 thruster pulses. The spacecraft enters its final limit cycle with an accuracy of below 0.8 degrees after approximately 7500 s, being a soft limit cycle about the body z-axis and a hard limit cycle about the satellite's y- and x-axis. This stabilisation averages about 245 thruster pulses per orbit for all three axes.
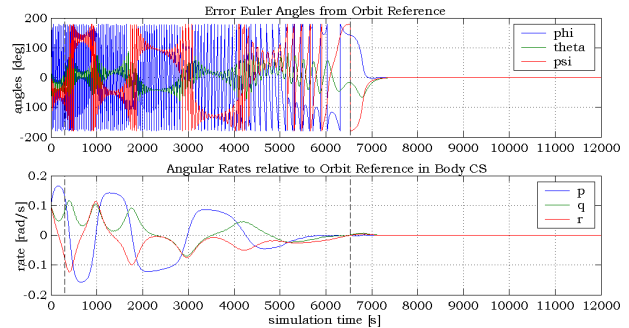


FIG. 14: Error Euler angles and body rates for complete CASsat mission scenario, 4-Force PPT, simulation with disturb. torques

## 5.2 SSETI EXPRESS Simulation

The main objective of this simulation was to show the versatility and functionality of the simulator as well as the controller design approaches for a new satellite, orbit and thruster system.

The detumbling controller achieves successful damping of the body rates to below 0.001 rad/s after about 20 s in a very fast detumbling process without any overshoot due to the high torque capabilities of the propulsion system.

The disturbing torque generated by the permanent magnet on board the SSETI EXPRESS spacecraft is very large, resulting in many thruster actuations for attitude stabilisation in nadir pointing mode. This long-term stability was therefore not investigated, instead the propulsion system is used for short-duration pointing manoeuvres for imaging with the camera.
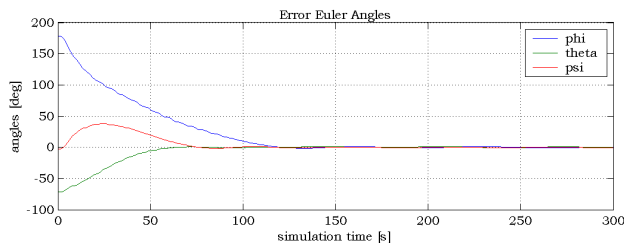


FIG. 15: Error Euler angles for acquisition manoeuvre using a quadratic switching function on SSETI EXPRESS

A quadratic switching function clearly shows the best performance for this application because of the minimum acquisition time. The reference attitude is reached after only 118 s (FIG. 15) with a total propellant consumption of 33.4 g. This simulation clearly shows that the SSETI EXPRESS cold gas propulsion unit is capable of 3-axis attitude control even with high disturbing environmental torques.

## 6 SUMMARY

A capable, modular and versatile simulation environment in Matlab/Simulink has been developed for full orbit and attitude motion simulation in low Earth orbit. Using a graphical user interface different satellite missions, control strategies and actuator setups for active attitude control can be specified and investigated.

This was verified using the CASsat pico-satellite with different pulsed plasma thruster setups as well as the SSETI EXPRESS micro-satellite, using a four thruster cold gas propulsion system.

The overall presented scenario shows the possibility of full 3-axis control of the CASsat mission using the four thruster PPT system and a linear quadratic regulator design. Stability of the controllers has been shown as well as detumbling, attitude acquisition and stabilisation to well below the required accuracy for the radiometer payload. However, the feasibility especially in terms of the power demand on the CubeSat mission needs to be verified as soon as more detailed information on the available power system and components are available.

The SSETI EXPRESS satellite and its propulsion system allowed verification and testing of the simulator's versatility with respect to different mission parameters and the transferability of the control approaches and optimisation considerations to a different mission scenario.

## 7 BIBLIOGRAPHY

[1] J. Schlutz: *Attitude and Orbit Control of Small Satellites Using Thruster Systems.* Diploma Thesis, Institute of Flight Mechanics and Control, Universitaet Stuttgart, June 2005.

[2] D.A. Vallado: *Fundamentals of Astrodynamics and Applications.* McGraw-Hill, New York, USA, 1997.

[3] V.A. Chobotov: *Orbital Mechanics, Second Edition.* AIAA Education Series, Reston, Virginia, 1996.

[4] V.A. Chobotov: *Spacecraft Attitude Dynamics and Control.* Krieger Publishing Company, Malabar, Florida, 1991.

[5] W. Fichter: *Advanced Spacecraft Navigation and Control.* Lecture Notes, Institute of Flight Mechanics and Control, Universitaet Stuttgart, 2004.

[6] C. Rayburn, M. Campbell, W.A. Hoskins, R.J. Cassady: *Development of a Micro Pulsed Plasma Thruster for the Dawgstar Nanosatellite.* AIAA-2000-3256, Proceedings of the 2000 AIAA/ASME/SAE/ASEE Joint Propulsion Conference, Huntsville, Alabama, 2000.

[7] G.G. Spanjers: *New Satellite Propulsion System Has Mass Below 100 Grams.* PR-01-09, AFRL's Propulsion Directorate, Edwards AFB, California, December 2001.

[8] N.J. Russel: *Pulsed Plasma Thrusters: Micro-Propulsion for Small Spacecraft.* Bachelor Thesis, Australian Centre for Field Robotics, University of Sydney, 2004.

[9] J. Schaefer: *SSETI Express: Mission Description Document.* Draft 3, Student Space Exploration & Technology Initiative, Noordwijk, 2005.

[10] F. Renk: *Attitude Control for a Microsatellite Using Only Magnetic Coils and Target Pointing for Multiple Satellites.* Diploma Thesis, Institute of Flight Mechanics and Control, Universitaet Stuttgart, March 2005.

[11] T.C. Ruppin: *Simulation of the CASsat Satellite and Environment.* Bachelor Thesis, Australian Centre for Field Robotics, University of Sydney, 2004.

[12] T. Staebler: *Nichtlineare Regelung und Neuronale Netze.* Lecture Notes, Institute of Flight Mechanics and Control, Universitaet Stuttgart, 2004.

[13] K.H. Well, B. Kaempf: *Mehrgroessenregelung.* Lecture Notes, Institute of Flight Mechanics and Control, Universitaet Stuttgart, 2004.